A frequent PLCγ1 mutation in adult T-cell leukemia/lymphoma determines functional properties of the malignant cells

Christy Prawiro[1], Tom D Bunney[2], Charis Kampyli[2], Hiroko Yaguchi[1], Matilda Katan[2*] and Charles R M Bangham[1*]

[1]Department of Infectious Diseases, Faculty of Medicine, Imperial College London, London, UK.

[2]Institute of Structural and Molecular Biology, Division of Biosciences, University College London, London, UK.

*Corresponding authors: m.katan@ucl.ac.uk; c.bangham@imperial.ac.uk

ABSTRACT

Background

Development of adult T-cell leukemia/lymphoma (ATL) involves human T-cell leukemia virus type 1 (HTLV-1) infection and accumulation of somatic mutations. The most frequently mutated gene in ATL (36% of cases) is phospholipase C gamma1 (*PLCG1*). *PLCG1* is also frequently mutated in other T-cell lymphomas. However, the functional consequences of the *PLCG1* mutations in cancer cells have not been characterized.

Methods

We compared the activity of the wild-type PLCγ1 with that of a mutant carrying a hot-spot mutation of PLCγ1 (S345F) observed in ATL, both in cells and in cell-free assays. To analyse the impact of the mutation on cellular properties, we quantified cellular proliferation, aggregation, chemotaxis and apoptosis by live cell-imaging in an *S345F*$^{+}$ ATL-derived cell line (KK1) and a KK1 cell line in which we reverted the mutation to the wild-type sequence using CRISPR/Cas9 and homology-directed repair.

Findings

The PLCγ1 S345F mutation results in an increase of basal PLC activity *in vitro* and in different cell types. This higher basal activity is further enhanced by upstream signalling. Reversion of the S345F mutation in the KK1 cell line resulted in reduction of the PLC activity, lower rates of proliferation and aggregation, and a marked reduction in chemotaxis towards CCL22. The PLCγ1-pathway inhibitors ibrutinib and ritonavir reduced both the PLC activity and the tested functions of KK1 cells.

Interpretation

Consistent with observations from clinical studies, our data provide direct evidence that activated variants of the PLCγ1 enzyme contribute to the properties of the malignant T-cell clone in ATL.

Funding

MRC (UK) Project Grant (P028160)

KEYWORDS

Adult T-cell leukemia/lymphoma (ATL); Phospholipase C gamma1 (PLCγ1); cancer mutations; ATL – derived cell lines; CRISPR-Cas9 gene editing.

NTRODUCTION

Adult T-cell leukemia/lymphoma (ATL) is a malignancy of mature T cells caused by human T-cell leukemia virus type 1 (HTLV-1), a retrovirus that predominantly infects CD4+ T cells (1, 2). Primary infection with HTLV-1 is asymptomatic and is typically followed by a long period - often several decades - of clinical latency. The majority of HTLV-1-infected individuals remain asymptomatic carriers throughout their life. However, around 5% of HTLV-1-infected individuals develop ATL, an aggressive T cell malignancy that is usually highly refractory to treatment, with an average survival time of 9-13 months (3, 4).

In infected individuals, the HTLV-1 provirus is integrated in the T cell genome. Two proteins expressed by HTLV-1, Tax and HBZ, have been extensively studied for their roles in ATL pathogenesis (1, 2). Although Tax promotes growth and inhibits apoptosis, it is the main target of the cytotoxic T lymphocyte (CTL) response to the virus. Therefore, its expression is disadvantageous for survival of infected cells and is lost in about 50% of ATL cases. HBZ is expressed in all ATL cases, suggesting its function in the development or maintenance of ATL. It has been proposed that the two genes cooperate to maintain persistent replication of HTLV-1+ T cell clones. A current hypothesis is that this persistent replication of the long-lived clones leads to the accumulation of replicative somatic mutations, some of which can act as oncogenic drivers for ATL (5, 6).

A comprehensive insight into recurrent, putative oncogenic driver mutations in ATL has been obtained from a large (426 cases), integrated molecular study, including whole-exome sequencing (7). Frequent mutations were found in genes implicated in cell proliferation and different T cell specific functions, frequently affecting components of the T-cell antigen receptor (TCR) signalling pathway. In this study, the most frequently mutated gene (36%) was *PLCG1,* encoding phospholipase C gamma 1 (PLCγ1), a second-messenger-generating enzyme and a key component in the TCR signalling pathway. Subsequent genetic studies of ATL (8-10) and studies of other types of T-cell lymphoma (including cutaneous T cell lymphoma (CTCL), angioimmunoblastic lymphoma (AITL) and peripheral T cell lymphoma (PTCL)) (11-14) also reported a high proportion of *PLCG1* mutations. Most of the observed changes were point mutations, resulting in amino acid substitutions, including a hot-spot S345F mutation. Recently, it has been shown that mutations in *PLCG1* can be detected in HTLV-1+ T-cell clones some years before the ATL diagnosis (15), and that *PLCG1* alterations are more common in the leukemic form of ATL than the lymphomatous form (9). It has also been reported that mutations in *PLCG1*, discovered in T-cell lymphoma and other cancers, lead to enhanced activity of the PLCγ1 enzyme, assessed in standard PLC assays (16, 17). These observations suggested that the *PLCG1* mutations frequently found in cases of ATL are activating mutations.

PLCγ1 has an essential role in regulation of physiological responses of T cells (18, 19), including TCR-induced activation of several signalling molecules and transcription factors; T cell development, activation, and tolerance (20); IL-2 stimulated T-cell proliferation and migration; and chemokine-regulated cell migration and homing (21-23). The activation by PLCγ1 of TCR signalling involves several adapter proteins (including LAT, Gads and SLP-76) and phosphorylation by tyrosine kinases such as Itk (24-26).

In contrast to the comprehensive insights into functions of the wild-type PLCγ1 in T cells, little is known about the functional consequences of its variants with activating mutations discovered in ATL and related T-cell lymphoma. Initial studies of cells from cases of CTCL with mutations in *PLCG1* revealed strong NFAT nuclear immunostaining, suggesting a link between enhanced PLC activity and activation of this transcription factor. The link between the activated PLCγ1 variants and an increase in activity of transcription factors (NFAT, NFkB and AP-1) has also been shown in Jurkat T cells, following transient expression of the PLCγ1 variants (11, 27). However, the relevance of such changes for T-cell malignancies remains unclear, and requires studies of the impact of PLCγ1 variants on specific cellular functions in cancer cells harbouring these mutations.

In this study, we identified a single copy of the hot-spot PLCγ1 S345F mutation in an established ATL-derived cell line and performed single-nucleotide gene correction with CRISPR-Cas9-mediated homology-directed repair (HDR). We found that this reversion to the PLCγ1 wild type impairs key functional properties of the ATL cell line, including a high rate of proliferation and chemotaxis. These findings, together with the insights from inhibition of the PLCγ1 pathway in the ATL cell line, link the activation of PLCγ1 by mutations to functions important in ATL pathology.

METHODS

HTLV-1 infected and ATL cell lines

Cell lines derived from HTLV-1 carriers (CY-6, USH'2, UR1, OGF20, MKI-1 and KAW2), smouldering/indolent subtype ATL (EE8, OKA3, YGS13, JSH4, YK8 and HAM9) and acute ATL (KOB, KK1, SO4, LMY1, LMY2 and LMWT5), were cultured as previously described (28, 29) and used to prepare DNA samples. The samples and the KK1 cell line (https://web.expasy.org/cellosaurus/CVCL_X908), originally described by Yamada et al. (30), were provided by Dr. Hasegawa (Nagasaki University). The

data identifying mutations in *PLCG1,* following amplification of the cell line DNA by PCR and Sanger sequencing (CelloPub=CLPUB00592), were provided by Dr. Varsha Patel (King's College London).

Cell culture of ATL-cell lines and treatment

KK1 cells were cultured in complete medium: RPMI-1640 medium (Sigma-Aldrich) with added L-glutamine (Invitrogen), penicillin and streptomycin (Invitrogen), 20% fetal bovine serum (FBS) (Invitrogen) and 100 U/mL IL-2 (Miltenyi Biotec) at 37˚C, 5% CO_2. The medium was changed every 2-3 days. Cells were counted with a LUNA-FL™ Dual Fluorescence Cell Counter (Logos Biosystems). After electroporation, cells were cultured in the same medium but without antibiotics. Sorted single cells were maintained in RPMI-1640 supplemented with 10% human serum (RPMI/10) (Biowest S4190-100) and addition of phytohemagglutinin (PHA) (Roche) once every two weeks. For treatment with small-molecule inhibitors, 1x10^6 cells were seeded in T25 flasks one day before the treatment. On the day of the treatment, medium was changed and replaced with normal medium supplemented with either 50μm ritonavir (Sigma-Aldrich) or 10μm ibrutinib (Sigma-Aldrich) for 24h. After the treatment, cells were washed once with RPMI-1640 medium before any experiment.

Genotyping

Genomic DNA was extracted from PBMCs using a DNA blood extraction kit (Qiagen) according to the manufacturer's protocol and used for both sequencing and ddPCR. For sequencing, PCR amplification was done using Phusion Hot Start Flex DNA polymerase (NEB), purified using QIAquick PCR Purification Kit (Qiagen) columns, and sent for Sanger sequencing (Eurofins Genomics) with primer 5'-TTTGTCACCTTCCTGTTCTCC-3', according to the respective manufacturer's protocol. For ddPCR, the final reaction mixture volume consisted of DNA (concentration normalized to 5 ng/ul), ddPCR supermix for Probes (Bio-Rad), RPP30 reference probe in HEX (Bio-Rad), PLCG1 p.S345F mutation detection probe in FAM (Bio-Rad), wild-type locked nucleic acid (LNA) oligonucleotide, and HindIII. Each reaction was loaded into one well of an eight-well cartridge (Bio-Rad) with 70 μl of droplet generation oil (Bio-Rad). Each reaction was run in duplicate, and droplets were formed using a QX200 Droplet Generator (Bio-Rad). Droplets were transferred to a 96-well PCR plate and amplified using a conventional thermal cycler. The thermocycling protocol was: (1) 95°C - 10 min, (2) 94°C – 30 s, 58°C – 1 min, step repeated 40 times (3) 98°C – 10 min, (4) 4°C – hold. The PCR products were loaded on a QX200 Droplet Reader (Bio-Rad) and analysed using QuantaSoft software (Bio-Rad).

Genome editing and cloning

A Neon™ electroporation system (Thermo Fisher) 10 μl kit was used to performed CRISPR-Cas9 mediated Homology Direct Repair. The program used for electroporation of KK1 mutant cells was: 2150 V, 20 ms, 1 pulse. On the day of electroporation, a plate containing antibiotic-free medium was pre-warmed. Ribonucleoprotein (RNP) was prepared by 10 minutes' incubation of a 9:1 ratio of sgRNA:Cas9 (both purchased from Synthego) at room temperature. SgRNAs tested were as follows: (1) 5'- CCTATCCAGGTACCTGACCG -3' (PAM sequence GGG) and (2) 5'- CTCACTGAAGAACTGGTCCC -3' (PAM sequence CGG). The RNP complex was then electroporated into cells together with 10 nM ssDNA HDR template (Dharmacon). The sequence of the HDR template used was:

5' - CCCATCTGACCATACCTACCTGCCTCTCCTTGCCTATCCAGGTACCTGACAGGGGACCAGTTCTCCAG TGAGTCCTCCTTGGAAGCCTATGCTCGCTGCCTGCGGATGGGCTGTCG -3'.

Cell density was adjusted to 500 000 cells/well. Cells, RNP complex and ssDNA HDR template were mixed together, aspirated using the 10 μl Neon tip, and electroporated using the above program and according to the manufacturer's protocol. The cells were then immediately transferred to the plate containing pre-warmed medium and incubated at 37°C in 5% CO_2. Sequencing and ddPCR were carried out 9 days after electroporation. The sequencing results were analysed using ICE analysis software (Synthego). The ddPCR results were analysed using QuantaSoft software (Bio-Rad). The wells that showed the required nucleotide correction were further expanded. Each expanded culture was split into two groups, for freezing and cloning. For cloning, single cells were isolated by fluorescence-activated cell sorting (FACS) in 96-well plates containing irradiated PBMCs, and monitored for growth. Live-cell sorting was performed under containment level 3 (CL3) conditions (Chelsea and Westminster Hospital, London) using a BD FACSAria III cell sorter. Cells were washed once, stained with 1 μg/mL LIVE/DEAD Fixable Near-IR Dead Cell Stain (Thermo Fisher Scientific) for 5 minutes, then washed and resuspended in RPMI-1640 without phenol red (Thermo Fisher Scientific) supplemented with 2% FBS.

Live cell imaging

All live-imaging experiments were performed using the IncuCyte Live-Cell Analysis System S3 (Sartorius) live-cell imaging system. Standard cell-culture 96-well plates (Corning 2596) were used for proliferation, apoptosis and clumping assay. IncuCyte Clearview 96-Well Plate (Sartorius) were used for the chemotaxis assay. All plates were thinly coated with Corning® Matrigel® Growth Factor Reduced Phenol-red free (Corning) to promote cellular adherence for imaging, according to the manufacturer's protocol. Five thousand cells were seeded per well for each experiment and plated

according to the manufacturer's protocol. For proliferation and apoptosis experiments, complete medium was used without IL-2, to avoid extensive clumping. For apoptosis assays, IncuCyte Annexin V Red Dyes (Sartorius 4641) were added to the medium for detection of phosphatidylserine exposure. For clumping experiments, complete medium including IL-2 was used. For chemotaxis experiments, growth medium was used without serum to minimize proliferation, with or without the addition of 500 ng/mL recombinant human CCL22 (R&D systems 336-MD-025) in the bottom well to induce migration. Images were taken as phase contrast (for proliferation, clumping, chemotaxis assays) with the addition of red fluorescence for apoptosis assays. Images were analysed with the IncuCyte Live-Cell Analysis System (Sartorius) using separate modules: Basic Analyzer module for proliferation and clumping, Adherent Cell-by-Cell module for apoptosis, and IncuCyte Chemotaxis Analysis Software Module (Top) for chemotaxis.

Generation of stable HEK cells lines

Stable HEK293 cell lines constitutively expressing either hPLCγ1 WT or hPLCγ1 S345F were generated by transfecting the cells with either the lentiviral expression plasmid hPLCγ1 WT or the lentiviral expression plasmid hPLCγ1 S345F. For plasmid DNA transfection, cells were transfected with polyethyleneimine (PEI). In each 10 cm dish, a total of 5 µg of plasmid DNA was used with 30 µl of PEI. Cells were cultured at 37°C in 5% CO_2. Selection of the cells expressing the protein of interest was started 48 hours after transfection, in presence of 2 µg/mL puromycin in the culture medium, DMEM with high glucose (GIBCO, #31966-021), 10% FBS and 100 U/mL penicillin/streptomycin. Two weeks later, GFP-positive cells were selected using fluorescence-activated cell sorting. For optimal enrichment, the top 10% of fluorescent cells were collected in 10 cm dishes, filled with 10 mL serum- and antibiotic- containing culture medium per dish. Selected cells were then expanded. A similar expression levels of PLCγ1 were confirmed by western blotting, using anti-PLCγ1 antibody (Millipore, #05-163).

Measurement of PLC activity

Measurement of PLC activity in HEK 293 stable cell lines - was done using the IP-ONE assay according to the manufacturer's instructions (Cisbio) as described by Liu et al. for COS-7 cells (17). This HTRF assay is based on quantitation of IP1, derivative of the PLC product - IP3, that is stable in the presence of LiCl. Briefly, HEK293 cells constitutively expressing either hPLCγ1 WT or hPLCγ1 S345F were plated in a 96-well plate, each well containing 30,000 cells + 100 µl medium. The following day, the medium

was replaced by 100 µl medium containing 50 mM LiCl and the plate was incubated for 1-2 hours at 37°C and 5% CO_2. Then, the medium was replaced by 25 µl of STIM buffer and 25 µl of LYSIS buffer and the cell lysis proceeded for 30 min in an orbital shaker at room temperature. From each well, duplicate samples (each 7 µl) were transferred to a 384-well plate. Then, 1.5 µl of IP1-d2 and 1.5 µl of anti-IP1-cryptate were added to each well of the 384-well plate, the plate was sealed and incubated for 1 hour at room temperature. Light emission at 665 nm and 620 nm was quantified at PHERAstar Microplate Reader, followed by calculation of the 665 nm/620 nm ratio.

Measurement of PLC activity in KK1 cells - KK1 cells were washed once and seeded at a density of 360,000/well in 50 µl of medium. Each condition included 8 experimental replicates. The medium consists of normal culture media containing 275 mM LiCl with or without inhibitors. The plate was incubated for 1-2 hours at 37°C and 5% CO_2. Then, 25 µl of IP1 kit LYSIS buffer was added to each well, resuspended thoroughly and placed on ice prior to further processing. The amount of IP1 present in the cell lysates was determined using the IP-ONE assay as described in Liu et al. (17).

Protein purification and measurement of PLC activity *in vitro*

PLCγ1 proteins (the wild type and S345F variant) were expressed and purified as described in Le Huray *et al.* (31). The proteins were expressed in *E. coli* and purified by a combination of Ni^{2+}-chelating, heparin affinity and gel filtration chromatography. Proteins were concentrated to around 5 mg/mL in centrifugal concentrators (Amicon Ultra - Millipore), aliquoted, snap-frozen in liquid nitrogen and stored at -80°C. PLC-catalysed hydrolysis of phosphatidylinositol incorporated in liposomes was monitored by quantifying the production of inositol phosphate (IP_1) using the IPone kit (CisBio) in an endpoint assay format as described in Liu et al (17), using the following assay buffer: 20 mM HEPES.KOH, 70 mM KCl, 3 mM EGTA, 2.97 mM $CaCl_2$, 2 mM TCEP, 50 µg/mL fatty acid-free BSA, pH 7.0. Liposomes were prepared as outlined in Le Huray *et al.* (31) and stored at a final concentration of 2 mg/mL and were composed of 20% PS, 45% PE, 15% PC, 10% cholesterol, 5% sphingomyelin and 5 % phosphatidylinositol (PI).

Liposomes containing PI as outlined above were thawed, diluted to 0.2 mg/mL lipid in Assay Buffer and stored at room temperature. The PLC proteins were assayed at a final concentration of 200 nM in a total assay volume of 200 µL. Samples of 15 µL were removed at various time intervals and the reaction stopped by the addition of 20 µL of stop buffer (50 mM EGTA, 0.6% (w/v) sodium cholate, pH 8.0) and heat denaturation at 80°C for 2 minutes. The amount of IP_1 was quantified through the addition of a labelled IP_1 probe and an anti-IP_1 labelled cryptate antibody and monitored by HTRF as

outlined in the manufacturer's instructions. The amount of IP_1 produced was calculated by interpolation from a standard curve.

Statistics

Statistical analysis of data obtained by live cells imaging was performed using Microsoft Excel or GraphPad Prism (GraphPad Software). All conditions included at least 3 independent biological replicates. Data are shown as mean ± standard error of the mean (SEM). Student's t-test (two-tailed) was used to compare means between two different groups. Values were considered statistically significant at $P < 0.05$.

For PLC activity measurements in cells, at least 2 experimental and 3 biological replicates were analysed for each condition. The data are presented as the mean and SEM. For *in vitro* PLC activity measurements, each data point was collected in triplicate and presented as the mean and SEM.

RESULTS

***PLCG1* S345F hot-spot mutation and its conversion to the *PLCG1* wild-type in ATL cells**

Analysis of a panel of non-malignant HTLV-1-infected cell lines and ATL cell lines for mutations in *PLCG1* identified mutations previously found in ATL clinical samples (7) in 4 out of 6 acute ATL cell lines but not in any of the HTLV-1 carriers or the smouldering subtype of ATL (Table S1). The KK1 cell line, derived from a case of acute ATL, harbours a heterozygous mutation resulting in a S345F amino acid substitution in *PLCG1,* which is frequently observed in ATL (7). The KK1 cell line has been used as a model of late-stage ATL in many studies, including recent studies related to the maintenance of the ATL clone and identification of key ATL transcriptional networks (32, 33).

We confirmed the expected expression by KK1 cells of CD4, the IL-2 receptor CD25 and the CCR4 chemokine receptor by flow cytometry and immunostaining, and the presence of a single copy of *PLCG1* S345F mutation in these cells by DNA sequencing (Figures S1A, B and S2). Analyses of the phosphorylation status of PLCγ1, ERK and AKT at functionally critical residues showed that, under standard culturing conditions, KK1 cells have detectable phosphorylation of PLCγ1 and ERK while AKT appears to be unphosphorylated (Figure S1C).

Recent crystal structures of the wild-type autoinhibited PLCγ1 (Protein Database identities 7Z3J and 6PBC) provide a basis for mechanistic interpretation of disease-linked mutations. In the PLCγ1 structure, Ser345 is positioned at the autoinhibitory interface (Figure 1A, left panel). The only reported replacement of Ser345 is Phe; this substitution abolishes interaction with Tyr506 in the regulatory region, compromising autoinhibition and thus increasing PLC activity (Figure 1A, right panels). It is also possible that, in activated PLCγ1, the region on the catalytic TIM-barrel domain containing the Phe345 has a stronger interaction with the membrane or directly with the substrate, contributing further to an increase in hydrolysis of the membrane resident PIP_2 (31).

Consistent with the data showing an increase in PLC activity in standard cell-based assays following transient transfection (16, 17), we found that both the PLCγ1 S345F protein analysed *in vitro* and PLCγ1 S345F stably expressed in cells have higher PLC activity than the wild-type (Figure 1B).

To study the functional consequences of the *PLCG1* S345F mutation in the context of ATL, we corrected this mutation in KK1 cells using CRISPR/Cas9-mediated homology-directed repair (Figure 1 C). The corrected mutation was verified by ddPCR (Figure 1C and Figure S2) and sequencing (Figure S2). The resulting cell line, encoding the wild-type PLCγ1, was designated KK1-revertant (KK1r) and the original cell line, encoding the mutant, as KK1-mutant (KK1m). Bright-phase low-magnification microscopy showed no major morphological difference between KK1m and KK1r (Figure S2C).

Because of the difference in PLC activity between the PLCγ1 S345F variant and the wild type observed *in vitro* and in transfected cells (Figure 1B), we compared the PLC activity in KK1m (expressing PLCγ1 S345F variant) and KK1r (expressing PLCγ1 wild type) cell lines (Figure 1D). The cellular assay is based on production of the PLC-generated second messenger inositol-1,4,5 trisphosphate (IP_3) and its conversion to a stable inositol-1 monophosphate (IP_1). We found a major reduction in PLC activity in the KK1r cells, showing that the correction altered the activity PLCγ1 and its downstream signalling (Figure 1D).

Proliferation, apoptosis and aggregation of KK1m and KK1r cells

To investigate in real time and quantify the kinetics of both proliferation and apoptosis in the KK1m and KK1r populations, we used the IncuCyte™ ZOOM live imaging system (Figure 2A and B). We found that the proliferation rate was higher in KK1m than in KK1r cells (Figure 2A). Faster growth of KK1m cells was also observed in routine suspension culture.

The rate of cellular proliferation is often positively correlated with the rate of apoptosis (34). We therefore investigated whether KK1r cells, with their slower rate of proliferation, also showed a lower

rate of apoptosis. Initial assessment by bright-phase low-magnification microscopy showed fewer dying cells in the KK1r culture (~90% viability) than in the KK1m cell culture (~65% viability) (Figure S1C). Staining with Annexin V, a fluorescent marker of early apoptosis, further revealed that, under the same seeding cell density and culture conditions, the KK1r cells had a lower rate of apoptosis than the KK1m cells (Figure 2B).

Increased aggregation (clumping) of normal and leukemic T cells has also been correlated with higher rates of proliferation and is a common feature of T cells in culture (35). The clumping involves colony formation followed by progressive fusion of smaller cell aggregates. T-cell colony formation can be induced by IL-2; decreasing IL-2 inhibits normal T-cell colony growth (36). KK1 cells, which express the high-affinity IL-2 receptor CD25, were isolated and cultured in the presence of IL-2 (28-30) (Figure S1). PLCγ1 can be activated following IL-2 stimulation of T cells (21). We therefore quantified the rate of cell clumping of KK1m and KK1r cell lines, in real time, for up to 40 hr (Figure 2C). In initial experiments with KK1m cells, following the fusion of colonies, smaller cell clumps fused more readily to generate larger clumps in the presence of IL-2 than in its absence (Figure S3). When further analysed in the presence of IL-2, KK1m cells also showed much greater clumping than KK1r cells at earlier (20 hr) and later (40 hr) time points, indicating a role of PLCγ1 S345F in this process (Figure 2C). The observation of increased cell clumping is consistent with the observed faster proliferation rate of KK1m cells.

Rate of chemotaxis in KK1m and KK1r cell lines

Chemotaxis is an important feature of normal T cells and T-cell malignancies, regulating cell migration and tissue infiltration. ATL is characterized by the strong expression of the chemokine receptor CCR4; about 30% of ATL cases have gain-of-function mutations in the *CCR4* gene which inhibit receptor internalization after ligand binding (7, 37, 38). CCR4 expressed in KK1 cells (Figure S1) has been reported to harbour a Y338* mutation that could result in upregulation of CCR4-mediated signalling (33). It has also been shown that PLCγ1 contributes to responses triggered by chemokine receptors and, more generally, could play a role in metastasis (23, 39, 40). We therefore compared the impact of the PLCγ1 S345F variant on CCR4-mediated chemotaxis in the KK1m and KK1r cell lines.

To quantify the rate of chemotaxis of KK1m cells in response to a known CCR4 ligand, the chemokine CCL22, we first established the difference between movement due to chemoactivation (a random movement due to activation by the chemokine) and true chemotaxis (directional movement up a concentration gradient of the chemokine) (Figure S4). We compared the rate of movement of cells in response to CCL22 in both top and bottom wells (chemoactivation) with the rate in response to chemokine only in the bottom well (chemotaxis). The results showed a significant difference between

the chemotaxis and chemoactivation, demonstrating that the selected conditions resulted in true chemotaxis.

We compared the rate of chemotaxis of KK1m and KK1r cell lines over 10 hr, using the IncuCyte (Figure 3). CCL22 induced rapid chemotaxis in KK1m cells at 5 hr and 10 hr, whereas KK1r showed no significant chemotaxis within 10 hr (Figure 3A). Light microscopy also revealed that KK1m cells tended to accumulate around the migration holes in contrast to the KK1r cells, confirming that the observed reduction in confluence of KK1m cells in the top well was due to active migration towards the bottom well (Figure 3B). These observations are consistent with the notion that the mutated PLCγ1 plays an important part in signalling by CCR4 receptor in this ATL cell line.

The effect of inhibitors of the PLCγ1 pathway on PIP2 hydrolysis and KK1 functions linked to the PLCγ1 S345F variant

An increase in basal PLC activity caused either by the PLCγ1 S345F mutation or one of several other activating mutations is further enhanced following stimulation in standard cell-based assays, resulting in hyperactivation (16, 17). This hyperactivation is likely to be a consequence of cooperation between the impact of mutations on the autoinhibition and the steps involved in physiological activation that are partially preserved in these activated variants. In addition to a further increase in stimulated PLC activity of PLCγ1 S345F in a standard assay, we found that this variant can also be further activated *via* TCR, when expressed in Jurkat *PLCG1* KO cells (Figure S5). We therefore conclude that various signalling inputs involved in physiological stimulation of PLCγ1 in T cells could also substantially contribute to high PLC activity of PLCγ1 S345F observed in KK1m cells.

To corroborate the observation that cell stimulation further enhanced the activity of the mutant PLCγ1, we used two inhibitors, ibrutinib and ritonavir, which act respectively at two points upstream in the activation pathways of PLCγ1 in the T cell (Figure 4A). Ibrutinib potently inhibits Itk, a TEC family kinase critical for many functions of T cells and implicated in T-cell malignancies (41-43). The phosphorylation of PLCγ1 Tyr783 by Itk results in stimulation of its PLC activity. Ritonavir directly binds to the SH3 domain of PLCγ1, resulting in disruption of protein-protein interactions required for T-cell activation. For example, a direct interaction of the PLCγ1 SH3 domain with the CD95/Fas receptor in Th17 cells and subsequent PLC activation are inhibited by ritonavir; this inhibitor can have a similar effect on binding to important T-cell adapter proteins such as SLP-76, best characterized as a component of TCR signalling (44, 45). Following initial characterization in Jurkat cells (Figure 5S), we found that in KK1m cells the treatment with either ibrutinib or ritonavir strongly reduced the rate of inositol phosphate production (Figure 4B). These data suggest that both phosphorylation of PLCγ1 and

protein-protein interactions are important for the high levels of PLC activity of the PLCγ1 S345F variant in KK1m cells.

To test whether the reduction in PLC activity in KK1m cells caused by the inhibitors also affects functional properties of these cells, as observed for the reversion of the mutant PLCγ1 to the wild type, we compared KK1m and KK1r cell lines in the assays measuring the rate of cell clumping in the presence of IL-2 and the rate of chemotaxis towards CCL22. These two assays showed consistent large differences between KK1m and KK1r cells (Figures 2C and 3).

Ritonavir reduced the rate of clumping in both KK1m and KK1r cells, which became statistically significantly different from the untreated control in KK1m cells at later timepoints (40 hrs) (Figure 5A, left panel and Figure S6A). Similarly, both KK1m and KK1r cells treated with ibrutinib showed significantly less clumping than the respective untreated cells (Figure 5A, right panel and Figure S6B). We also measured the average object (clump) area at each time point: the results confirmed the observed differences in clumping between the two cell lines (Figure 5B). Individual untreated KK1m cells formed small colonies which fused over time, creating larger clumps, as shown by the increasing average object area. By contrast, although KK1r cells also formed small colonies, these colonies did not rapidly increase in size by colony fusion. Treatment with either ritonavir or ibrutinib significantly reduced the average object area in the KK1m culture to a value similar to that seen in the KK1r culture (Figure 5B and Figure S6C and D). Treatment of the KK1r cells with either drug abolished the ability to form colonies (Figure 5B).

We then tested the impact of treatment with either ritonavir or ibrutinib on the rate of chemotaxis of KK1m cells towards CCL22. Treatment with either drug led to a significant inhibition of chemotaxis, especially at the later times (10 hrs) (Figure 5C), although the effect of the drugs (especially ibrutinib; Figure S7) was weaker than that of reversion of PLCγ1 mutation in KK1r cells, which showed little or no chemotaxis (Figure 3). However, as in the assay of cell clumping, we observed a correlation between the reduction in PLC activity (Figure 4B) and the impairment of KK1m functions following the treatment with inhibitors (Figure 5); this observation is consistent with the correlation between PLC activity and KK1m functions shown in Figure 1D, Figure 2 and Figure 3.

DISCUSSION

While many genetic studies implicate mutations in the *PLCG1* gene as a potential oncogenic driver in ATL and other T-cell lymphomas (7-14), direct evidence that activated variants of the PLCγ1 enzyme contribute to the T-cell lymphoma pathology has been lacking. Here we show that the conversion of a mutated *PLCG1* gene to its wild type in ATL cells, and the inhibition of the PLCγ1 pathway, resulting in reduction of PLC activity, each have a profound effect on T cell functions important in the malignant phenotype of ATL.

Although cancer develops through progressive somatic mutations, with an average of 30-60 mutations capable of altering protein function in established cancers, comprehensive preclinical and clinical evidence suggests that cancer cells depend on relatively few genetic driver events (46-48). These findings enabled the discovery of agents for targeted cancer therapies, which, even as single agents, have prolonged the lives of many cancer patients (49, 50). Recent studies have provided comprehensive analyses of the genetic changes in ATL and other T-cell malignancies with an unmet clinical need (7-14).

Since activating mutations in *PLCG1* are the most frequent mutations observed in ATL, and also occur in other types of T-cell lymphoma, it is important to assess whether these mutations can cause or maintain properties of the malignant phenotype. In the absence of reliable direct pharmacological PLC inhibitors, we used CRISPR/Cas9 to revert a known hot-spot mutation in *PLCG1* (resulting in the S345F substitution) to the wild type in an established acute ATL-derived cell line, KK1, resulting in the reduction of PLC activity in these cells (Figure 1). Although this reversion did not cause cell death, the high rates observed in KK1 cells of cell proliferation and chemotaxis, which are important for cancer progression and spreading, were greatly reduced (Figures 2 and 3). Initial studies of the clinical importance of *PLCG1* mutations have shown that the mutations found in diagnostic CTCL samples persisted in multiple tumour compartments over time (27) and that the frequent S345F substitution is associated with a lower overall survival in PTCL-NOS (51). Similar findings have been reported in a recent longitudinal study of cases of aggressive ATL, progressing from indolent subtypes (10). The data showed an enrichment in mutations in pathways involving *PLCG1,* TCR, and NF-κB in aggressive subtypes, arising from rare pre-existing subclones found in both the original tumour at the indolent stage and the relapsed cases. The same study (10) also reported a correlation between these mutations and a significantly shorter time to progression and lower overall survival. In an earlier report, *PLCG1* mutations were identified in indolent and aggressive subtypes of ATL (52). Our present findings, showing the requirement for the mutated form of PLCγ1 for high rates of proliferation and chemotaxis of KK1 cells (Figures 2 and 3), are consistent with the studies of T-cell lymphoma (7-14)

and suggest an important contribution of the upregulated PLCγ1 activity in the development and persistence of malignant properties. In ATL, the mutated variants of PLCγ1 may synergize with various Tax-protein-induced host proteins that enhance proliferation, conferring a survival and growth advantage on the malignant clone (5, 7, 15).

Constitutively activated mutants of PLCγ1 can disrupt many cellular functions that are regulated by PLCγ1 as a key component of intracellular signalling linked to cell surface receptors (20). Mutations such as the S345F substitution not only enhance the basal activity of the enzyme but also result in hyperactivation in response to stimulation, causing potential upregulation of functional responses to extracellular stimuli ((16, 17) and Figure S5). In the KK1 cell line, the deregulated signalling pathways are likely to include the TCR pathway, which is frequently highly phosphorylated and upregulated in T-cell lymphoma (as documented in AITL (42)), and the pathways triggered by other receptors such as CD25 and chemokine receptors (21, 23). A number of agonists can regulate the rates of proliferation and migration of ATL cell lines, and we show here that cell aggregation (which correlates with the proliferation rate) in response to the CD25 ligand, IL-2, is greatly reduced in revertant KK1 cells expressing the PLCγ1 wild type (KK1r) (Figure 2). A high rate of chemotaxis towards CCL22, mediated by the CCR4 receptor, similarly depends on the mutated variant of PLCγ1 in KK1 cells (Figure 3). The inhibitor of the upstream kinase Itk, ibrutinib, and a compound blocking certain PLCγ1 protein-protein interactions, ritonavir, reduced the PLC activity and functional responses in KK1 cells (Figures 4 and 5). These observations are consistent with the results of reversion of the PLCγ1 activating mutation (Figures 1-3), confirming an association between the enhanced PLC activity and the magnitude of the response in each functional assay (Figures 4 and 5). These data also demonstrate the contribution of phosphorylation and binding of regulatory proteins to the hyperactivated state of the PLCγ1 S345F variant in KK1 cells.

Identification of the consequences of the molecular changes in ATL has stimulated efforts to test and develop new treatments, including strategies targeted to components of the TCR-NF-κB pathway, regulation of chemotaxis and immune evasion (4, 53, 54). An anti-CCR4 monoclonal antibody, mogamulizumab, has had some success in clinical trials and has been approved for the treatment of the relapsed, refractory ATL in Japan (55, 56). Other putative targets (including IRF4 transcription factor and PI-3 kinase) are also being assessed in clinical trials (53). Among the proteins in the TCR-NFkB pathway in ATL, PKCβ and MALT1 have been considered as therapeutic targets (53). In other types of T-cell lymphoma, several reports related to targeting of the TCR pathway highlighted both the potential and the shortcomings of ibrutinib, which targets Itk in T cells; Itk is also essential for chemokine-induced migration (42, 43, 57). The results presented here and previously reported data from genetic analyses (7-10) suggest that *PLCG1* mutations should be included as predictive markers

of ATL and identify the activated variants of PLCγ1 as a potential therapeutic target. For this purpose, new candidate PLCγ1 inhibitors must be tested for their ability to alter T cell function in a wider range of ATL cells; such direct PLC inhibitors may subsequently be developed for clinical applications. Since PLCγ enzymes are implicated in several types of disease (19, 58) as well as T cell malignancies, these efforts are likely to have broader impact by focusing on this so far unexploited target.

Contributors

Conceptualization: CRMB, MK, TDB

Methodology development and conducting the experiments: CP, TDB, CK, HY

Analysing and assessing data: CP, TDB, CK, CRMB, MK

Writing the original draft: CP, MK

Review & editing of the manuscript: CRMB, TDB, CK

Decision to submit the manuscript: CRMB, MK

All authors read and approved the final version of this manuscript.

Declaration of Interests

All authors have nothing to disclose.

Acknowledgments

This work was supported by the Medical Research Council (MRC) Project Grant (P028160) to MK and CRMB.

Data Sharing Statement

All original data are available on request from the corresponding authors.

Supplementary materials

Supplementary materials are associated with this article.

REFERENCES

1. Bangham CRM. Human T Cell Leukemia Virus Type 1: Persistence and Pathogenesis. Annu Rev Immunol. 2018;36:43-71.

2. Watanabe T. Adult T-cell leukemia: molecular basis for clonal expansion and transformation of HTLV-1-infected T cells. Blood. 2017;129(9):1071-81.

3. Cook L, Rowan A, Bangham C. Adult T-cell leukemia/lymphoma—pathobiology and implications for modern clinical management. Annals of Lymphoma. 2021;5:1-10.

4. Cook LB, Fuji S, Hermine O, Bazarbachi A, Ramos JC, Ratner L, et al. Revised Adult T-Cell Leukemia-Lymphoma International Consensus Meeting Report. J Clin Oncol. 2019;37(8):677-87.

5. Bangham CRM, Matsuoka M. Human T-cell leukaemia virus type 1: parasitism and pathogenesis. Philos Trans R Soc Lond B Biol Sci. 2017;372(1732).

6. Tomasetti C, Li L, Vogelstein B. Stem cell divisions, somatic mutations, cancer etiology, and cancer prevention. Science. 2017;355(6331):1330-4.

7. Kataoka K, Nagata Y, Kitanaka A, Shiraishi Y, Shimamura T, Yasunaga J, et al. Integrated molecular analysis of adult T cell leukemia/lymphoma. Nat Genet. 2015;47(11):1304-15.

8. Sakihama S, Morichika K, Saito R, Miyara M, Miyagi T, Hayashi M, et al. Genetic profile of adult T-cell leukemia/lymphoma in Okinawa: Association with prognosis, ethnicity, and HTLV-1 strains. Cancer Sci. 2021;112(3):1300-9.

9. Kogure Y, Kameda T, Koya J, Yoshimitsu M, Nosaka K, Yasunaga JI, et al. Whole-genome landscape of adult T-cell leukemia/lymphoma. Blood. 2022;139(7):967-82.

10. Marcais A, Lhermitte L, Artesi M, Laurent C, Durkin K, Hahaut V, et al. Targeted deep sequencing reveals clonal and subclonal mutational signatures in Adult T-cell leukemia/lymphoma and defines an unfavorable indolent subtype. Leukemia. 2021;35(3):764-76.

11. Vaque JP, Gomez-Lopez G, Monsalvez V, Varela I, Martinez N, Perez C, et al. PLCG1 mutations in cutaneous T-cell lymphomas. Blood. 2014;123(13):2034-43.

12. da Silva Almeida AC, Abate F, Khiabanian H, Martinez-Escala E, Guitart J, Tensen CP, et al. The mutational landscape of cutaneous T cell lymphoma and Sezary syndrome. Nat Genet. 2015;47(12):1465-70.

13. Vallois D, Dobay MP, Morin RD, Lemonnier F, Missiaglia E, Juilland M, et al. Activating mutations in genes related to TCR signaling in angioimmunoblastic and other follicular helper T-cell-derived lymphomas. Blood. 2016;128(11):1490-502.

14. Manso R, Gonzalez-Rincon J, Rodriguez-Justo M, Roncador G, Gomez S, Sanchez-Beato M, et al. Overlap at the molecular and immunohistochemical levels between angioimmunoblastic T-cell

lymphoma and a subgroup of peripheral T-cell lymphomas without specific morphological features. Oncotarget. 2018;9(22):16124-33.

15. Rowan AG, Dillon R, Witkover A, Melamed A, Demontis MA, Gillet NA, et al. Evolution of retrovirus-infected premalignant T-cell clones prior to adult T-cell leukemia/lymphoma diagnosis. Blood. 2020;135(23):2023-32.

16. Hajicek N, Keith NC, Siraliev-Perez E, Temple BR, Huang W, Zhang Q, et al. Structural basis for the activation of PLC-gamma isozymes by phosphorylation and cancer-associated mutations. Elife. 2019;8.

17. Liu Y, Bunney TD, Khosa S, Mace K, Beckenbauer K, Askwith T, et al. Structural insights and activating mutations in diverse pathologies define mechanisms of deregulation for phospholipase C gamma enzymes. EBioMedicine. 2020;51:102607.

18. Brownlie RJ, Zamoyska R. T cell receptor signalling networks: branched, diversified and bounded. Nat Rev Immunol. 2013;13(4):257-69.

19. Katan M, Cockcroft S. Phospholipase C families: Common themes and versatility in physiology and pathology. Prog Lipid Res. 2020;80:101065.

20. Fu G, Chen Y, Yu M, Podd A, Schuman J, He Y, et al. Phospholipase C{gamma}1 is essential for T cell development, activation, and tolerance. J Exp Med. 2010;207(2):309-18.

21. Llavero F, Artaso A, Lacerda HM, Parada LA, Zugaza JL. Lck/PLCgamma control migration and proliferation of interleukin (IL)-2-stimulated T cells via the Rac1 GTPase/glycogen phosphorylase pathway. Cell Signal. 2016;28(11):1713-24.

22. de Gorter DJ, Beuling EA, Kersseboom R, Middendorp S, van Gils JM, Hendriks RW, et al. Bruton's tyrosine kinase and phospholipase Cgamma2 mediate chemokine-controlled B cell migration and homing. Immunity. 2007;26(1):93-104.

23. Shannon LA, Calloway PA, Welch TP, Vines CM. CCR7/CCL21 migration on fibronectin is mediated by phospholipase Cgamma1 and ERK1/2 in primary T lymphocytes. J Biol Chem. 2010;285(50):38781-7.

24. Huse M. The T-cell-receptor signaling network. J Cell Sci. 2009;122(Pt 9):1269-73.

25. Manna A, Zhao H, Wada J, Balagopalan L, Tagad HD, Appella E, et al. Cooperative assembly of a four-molecule signaling complex formed upon T cell antigen receptor activation. Proc Natl Acad Sci U S A. 2018;115(51):E11914-E23.

26. Wada J, Rathnayake U, Jenkins LM, Singh A, Mohammadi M, Appella E, et al. In vitro reconstitution reveals cooperative mechanisms of adapter protein-mediated activation of phospholipase C-gamma1 in T cells. J Biol Chem. 2022;298(3):101680.

27. Patel VM, Flanagan CE, Martins M, Jones CL, Butler RM, Woollard WJ, et al. Frequent and Persistent PLCG1 Mutations in Sezary Cells Directly Enhance PLCgamma1 Activity and Stimulate NFkappaB, AP-1, and NFAT Signaling. J Invest Dermatol. 2020;140(2):380-9 e4.

28. Hata T, Fujimoto T, Tsushima H, Murata K, Tsukasaki K, Atogami S, et al. Multi-clonal expansion of unique human T-lymphotropic virus type-I-infected T cells with high growth potential in response to interleukin-2 in prodromal phase of adult T cell leukemia. Leukemia. 1999;13(2):215-21.

29. Fujimoto T, Hata T, Itoyama T, Nakamura H, Tsukasaki K, Yamada Y, et al. High rate of chromosomal abnormalities in HTLV-I-infected T-cell colonies derived from prodromal phase of adult T-cell leukemia: a study of IL-2-stimulated colony formation in methylcellulose. Cancer Genet Cytogenet. 1999;109(1):1-13.

30. Yamada Y, Nagata Y, Kamihira S, Tagawa M, Ichimaru M, Tomonaga M, et al. IL-2-dependent ATL cell lines with phenotypes differing from the original leukemia cells. Leuk Res. 1991;15(7):619-25.

31. Le Huray KIP, Bunney TD, Pinotsis N, Kalli AC, Katan M. Characterization of the membrane interactions of phospholipase Cgamma reveals key features of the active enzyme. Sci Adv. 2022;8(25):eabp9688.

32. Mahgoub M, Yasunaga JI, Iwami S, Nakaoka S, Koizumi Y, Shimura K, et al. Sporadic on/off switching of HTLV-1 Tax expression is crucial to maintain the whole population of virus-induced leukemic cells. Proc Natl Acad Sci U S A. 2018;115(6):E1269-E78.

33. Nakagawa M, Shaffer AL, 3rd, Ceribelli M, Zhang M, Wright G, Huang DW, et al. Targeting the HTLV-I-Regulated BATF3/IRF4 Transcriptional Network in Adult T Cell Leukemia/Lymphoma. Cancer Cell. 2018;34(2):286-97 e10.

34. Fogarty CE, Bergmann A. Killers creating new life: caspases drive apoptosis-induced proliferation in tissue repair and disease. Cell Death Differ. 2017;24(8):1390-400.

35. Magistroni R, Mangolini A, Guzzo S, Testa F, Rapana MR, Mignani R, et al. TRPP2 dysfunction decreases ATP-evoked calcium, induces cell aggregation and stimulates proliferation in T lymphocytes. BMC Nephrol. 2019;20(1):355.

36. Lunardi-Iskandar Y, Georgoulias V, Vittecoq D, Nugeyre MT, Ammar A, Clemenceau C, et al. Peripheral blood adherent cells from AIDS patients inhibit normal T-colony growth through decreased expression of interleukin 2-receptors and production of interleukin 2. Leuk Res. 1987;11(8):753-60.

37. Yoshie O, Fujisawa R, Nakayama T, Harasawa H, Tago H, Izawa D, et al. Frequent expression of CCR4 in adult T-cell leukemia and human T-cell leukemia virus type 1-transformed T cells. Blood. 2002;99(5):1505-11.

38. Nakagawa M, Schmitz R, Xiao W, Goldman CK, Xu W, Yang Y, et al. Gain-of-function CCR4 mutations in adult T cell leukemia/lymphoma. J Exp Med. 2014;211(13):2497-505.

39. Wang J, Zhang X, Thomas SM, Grandis JR, Wells A, Chen ZG, et al. Chemokine receptor 7 activates phosphoinositide-3 kinase-mediated invasive and prosurvival pathways in head and neck cancer cells independent of EGFR. Oncogene. 2005;24(38):5897-904.

40. Sala G, Dituri F, Raimondi C, Previdi S, Maffucci T, Mazzoletti M, et al. Phospholipase Cgamma1 is required for metastasis development and progression. Cancer Res. 2008;68(24):10187-96.

41. Dubovsky JA, Beckwith KA, Natarajan G, Woyach JA, Jaglowski S, Zhong Y, et al. Ibrutinib is an irreversible molecular inhibitor of ITK driving a Th1-selective pressure in T lymphocytes. Blood. 2013;122(15):2539-49.

42. Liu Y, Wang X, Deng L, Ping L, Shi Y, Zheng W, et al. ITK inhibition induced in vitro and in vivo anti-tumor activity through downregulating TCR signaling pathway in malignant T cell lymphoma. Cancer Cell Int. 2019;19:32.

43. Mamand S, Allchin RL, Ahearne MJ, Wagner SD. Comparison of interleukin-2-inducible kinase (ITK) inhibitors and potential for combination therapies for T-cell lymphoma. Sci Rep. 2018;8(1):14216.

44. Poissonnier A, Guegan JP, Nguyen HT, Best D, Levoin N, Kozlov G, et al. Disrupting the CD95-PLCgamma1 interaction prevents Th17-driven inflammation. Nat Chem Biol. 2018;14(12):1079-89.

45. Tripathi N, Vetrivel I, Teletchea S, Jean M, Legembre P, Laurent AD. Investigation of Phospholipase Cgamma1 Interaction with SLP76 Using Molecular Modeling Methods for Identifying Novel Inhibitors. Int J Mol Sci. 2019;20(19).

46. Vogelstein B, Papadopoulos N, Velculescu VE, Zhou S, Diaz LA, Jr., Kinzler KW. Cancer genome landscapes. Science. 2013;339(6127):1546-58.

47. Weinstein IB, Joe A. Oncogene addiction. Cancer Res. 2008;68(9):3077-80; discussion 80.

48. Luo J, Solimini NL, Elledge SJ. Principles of cancer therapy: oncogene and non-oncogene addiction. Cell. 2009;136(5):823-37.

49. Bedard PL, Hyman DM, Davids MS, Siu LL. Small molecules, big impact: 20 years of targeted therapy in oncology. Lancet. 2020;395(10229):1078-88.

50. Cohen P, Cross D, Janne PA. Kinase drug discovery 20 years after imatinib: progress and future directions. Nat Rev Drug Discov. 2021;20(7):551-69.

51. Manso R, Rodriguez-Pinilla SM, Gonzalez-Rincon J, Gomez S, Monsalvo S, Llamas P, et al. Recurrent presence of the PLCG1 S345F mutation in nodal peripheral T-cell lymphomas. Haematologica. 2015;100(1):e25-7.

52. Kataoka K, Iwanaga M, Yasunaga JI, Nagata Y, Kitanaka A, Kameda T, et al. Prognostic relevance of integrated genetic profiling in adult T-cell leukemia/lymphoma. Blood. 2018;131(2):215-25.

53. Yoshida N, Miyoshi H, Ohshima K. Clinical Applications of Genomic Alterations in ATLL: Predictive Markers and Therapeutic Targets. Cancers (Basel). 2021;13(8).

54. El Hajj H, Tsukasaki K, Cheminant M, Bazarbachi A, Watanabe T, Hermine O. Novel Treatments of Adult T Cell Leukemia Lymphoma. Front Microbiol. 2020;11:1062.

55. Yamamoto K, Utsunomiya A, Tobinai K, Tsukasaki K, Uike N, Uozumi K, et al. Phase I study of KW-0761, a defucosylated humanized anti-CCR4 antibody, in relapsed patients with adult T-cell leukemia-lymphoma and peripheral T-cell lymphoma. J Clin Oncol. 2010;28(9):1591-8.

56. Ishida T, Joh T, Uike N, Yamamoto K, Utsunomiya A, Yoshida S, et al. Defucosylated anti-CCR4 monoclonal antibody (KW-0761) for relapsed adult T-cell leukemia-lymphoma: a multicenter phase II study. J Clin Oncol. 2012;30(8):837-42.

57. Kumar A, Vardhana S, Moskowitz AJ, Porcu P, Dogan A, Dubovsky JA, et al. Pilot trial of ibrutinib in patients with relapsed or refractory T-cell lymphoma. Blood Adv. 2018;2(8):871-6.

58. Koss H, Bunney TD, Behjati S, Katan M. Dysfunction of phospholipase Cgamma in immune disorders and cancer. Trends Biochem Sci. 2014;39(12):603-11.

FIGURE LEGENDS

Figure 1. The S345F mutation lies at the autoinhibitory interface of PLCγ1 and contributes to high PLC activity in KK1m cells. (A) Structural model of PLCγ1 (based on PDB ID 7Z3J), showing the PLC-core (dark blue), regulatory γ-SA (light blue) and autoinhibitory interfaces (1 and 2, red). Position of S345 is indicated. A close-up view of the S345 amino acid residue that forms a hydrogen bond with Y509. The corresponding mutated F345 residue does not form a hydrogen bond; one possible orientation of F345 is shown, based on analyses by program Modeller 10.3 (right panels). **(B)** PLC activity, assessed by generation of IP1, of PLCγ1 WT and PLCγ1 S345F variant, measured in a liposome assay *in vitro* (left panel) and in stably transfected HEK293 cell lines, under basal conditions in the presence of LiCl for 1h (right panel). **(C)** A 1-dimensional ddPCR profile representing four samples: a normal T-cell clone 11.65, KK1 mutant (KK1m), KK1 revertant (KK1r), and a control NFW (nuclease-free water). The yellow lines represent a duplicate run of the same sample. The top panel shows S345F mutation (blue droplets), and the bottom panel shows the ubiquitous housekeeping gene, RPP30 (green droplets). Amplitude threshold is represented with a pink line. **(D)** Measurement of PLC activity, by generation of IP1, in KK1m (with mutated PLCγ1) and KK1r (with corrected PLCγ1) cell lines in the presence of LiCl for 1h. Values for all measurements of PLC activity are presented as the mean and SEM.

Figure 2. Higher rates of proliferation, apoptosis and clumping in KK1 mutant (KK1m) compared to the KK1 revertant (KK1r) cells. In each panel (A to C), the bar-chart (right-hand side) shows the statistical analysis at the beginning (t=0h), middle (t=20h), and end (t=40h) of the experiment. **(A)** Representative timecourse of proliferation (n=5), showing the total confluency measured in phase-contrast over 40 hr, normalized to % confluence at t=0. **(B)** Representative timecourse of apoptosis (Annexin V+ intensity) over 10 hr, normalized to Annexin V intensity at t=0; (n=3). **(C)** Representative timecourse of clumping (confluence) (n=3) over 40 hr, normalized to total clump area at t=0. Representative images of KK1mut and KK1rev at t=40h are shown in the bottom panel. Clumping experiments were carried out in complete media, in the presence of IL-2 (100 U/mL). Parametric t-test was used to calculate significant difference. *P* values are indicated by asterisks as follows: **** = $P < 0.0001$, *** = *P* 0.0001 to 0.001, ** = *P* 0.001 to 0.01 and * = *P* 0.01 to 0.05; $P \geq 0.05$ is not significant and not noted.

Figure 3. Chemotaxis occurs at much higher rate in KK1 mutant (KK1m) compared to the KK1 revertant (KK1r). (A) Representative timecourse of chemotaxis over 10 hr, quantified as % confluence of cells in the top well, normalized to % confluence at t=0 (left panel). Recombinant human CCL22 (500 ng/mL) was added in the bottom well to induce migration. Statistical analysis of the chemotaxis timecourse replicates (n=3) at the beginning (t=0h), middle (t=5h), and end (t=10h) of the experiment (right panel). Significant differences are calculated and indicated by asterisks as in Figure 2. **(B)** Representative images of KK1m and KK1r cell in the top well at t=10h.

Figure 4. Inhibition of key regulators of PLCγ1 signalling. (A) Inhibition of PLCγ1 signalling by ibrutinib and ritonavir. Individual domains in PLCγ1 are labelled and the PLC-core and regulatory region shown in dark and light blue, respectively. Following engagement of the TCR, many downstream components become phosphorylated, including an adapter protein LAT which, together with other adapters, Gads and SLP-76, forms a membrane-proximal complex with PLCγ1 (pLAT/Gads/SLP-76/PLCγ1 signalling complex). Activation of PLCγ1 further requires phosphorylation of Tyr783 in the regulatory region, by the Itk kinase. Receptors other than TCR, including CD25 and chemokine receptors, can activate kinases such as Lck and Itk, that contribute to activation of PLCγ1. The inhibition of Itk by ibrutinib abolishes phosphorylation and activation of PLCγ1. Another inhibitor, ritonavir, directly binds to PLCγ1 and so prevents binding of SLP-76 to the SH3 domain of PLCγ1; consequently, this inhibition can compromise formation of signalling complexes involved in activation of PLCγ1. Chemical structures of

the inhibitors are shown, and their protein targets (red arrows) and processes affected (red crosses) indicated. **(B)** Measurement of PLC activity by IP1 assay (as described in Figure 1D) in KK1m cells without a treatment, KK1m cells treated with ibrutinib (10μM) and KK1m cells treated with ritonavir (50μM) for 24h.

Figure 5. Effect of ritonavir and ibrutinib on cell clumping and chemotaxis. (A) Mean rate of clumping (n=4), in the presence of 100 U/mL IL-2, of KK1m and KK1r lines at the beginning (t=0h), middle (t=20h), and end (t=40h) of the timecourse, normalized to t=0, with or without ritonavir (left panel) or ibrutinib (IB) (right panel). **(B)** As in (A) but measuring the average object area of the clumps with and without ritonavir (RITO) (left panel) or ibrutinib (IB) (right panel). **(C)** Mean rate of chemotaxis (n=3), induced by 500 ng/mL CCL22, of KK1m cells with and without ritonavir (RITO) (left panel) or ibrutinib (IB) (right panel) at the beginning (t=0h), middle (t=5h), and end (t=10h) of the timecourse, normalized to t=0. Significant differences are calculated and indicated by asterisks as in Figure 2.

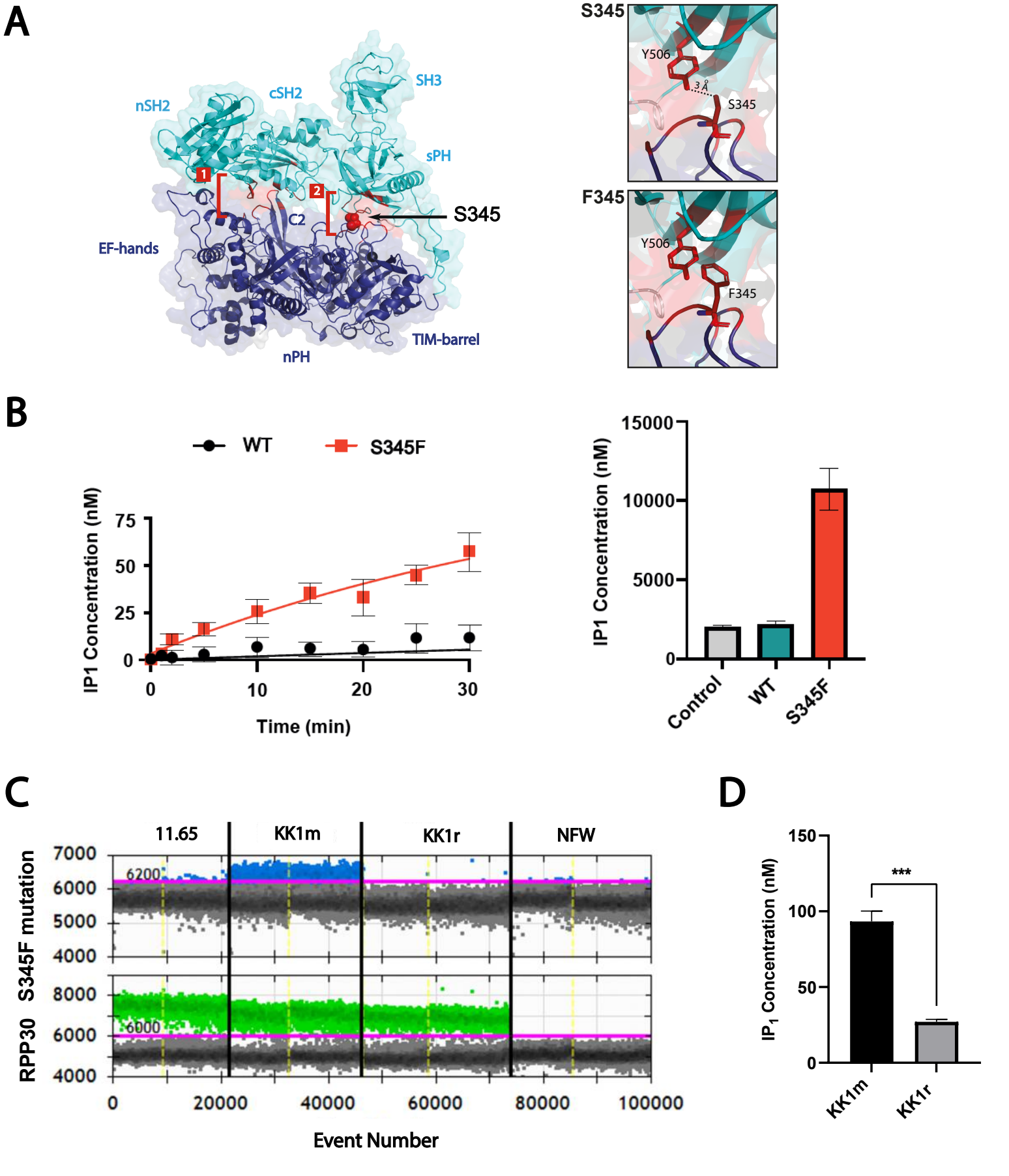
A
nSH2
cSH2
SH3
sPH
C2
EF-hands
S345
TIM-barrel
nPH
S345
Y506
3 Å
S345
F345
Y506
F345
B
WT
S345F
IP1 Concentration (nM)
75
50
25
0
0
10
20
30
Time (min)
IP1 Concentration (nM)
15000
10000
5000
0
Control
WT
S345F
C
11.65
KK1m
KK1r
NFW
S345F mutation
RPP30
7000
6000
5000
4000
6200
8000
6000
4000
6000
0
20000
40000
60000
80000
100000
Event Number
D
IP1 Concentration (nM)
150
100
50
0
***
KK1m
KK1r

Figure 1

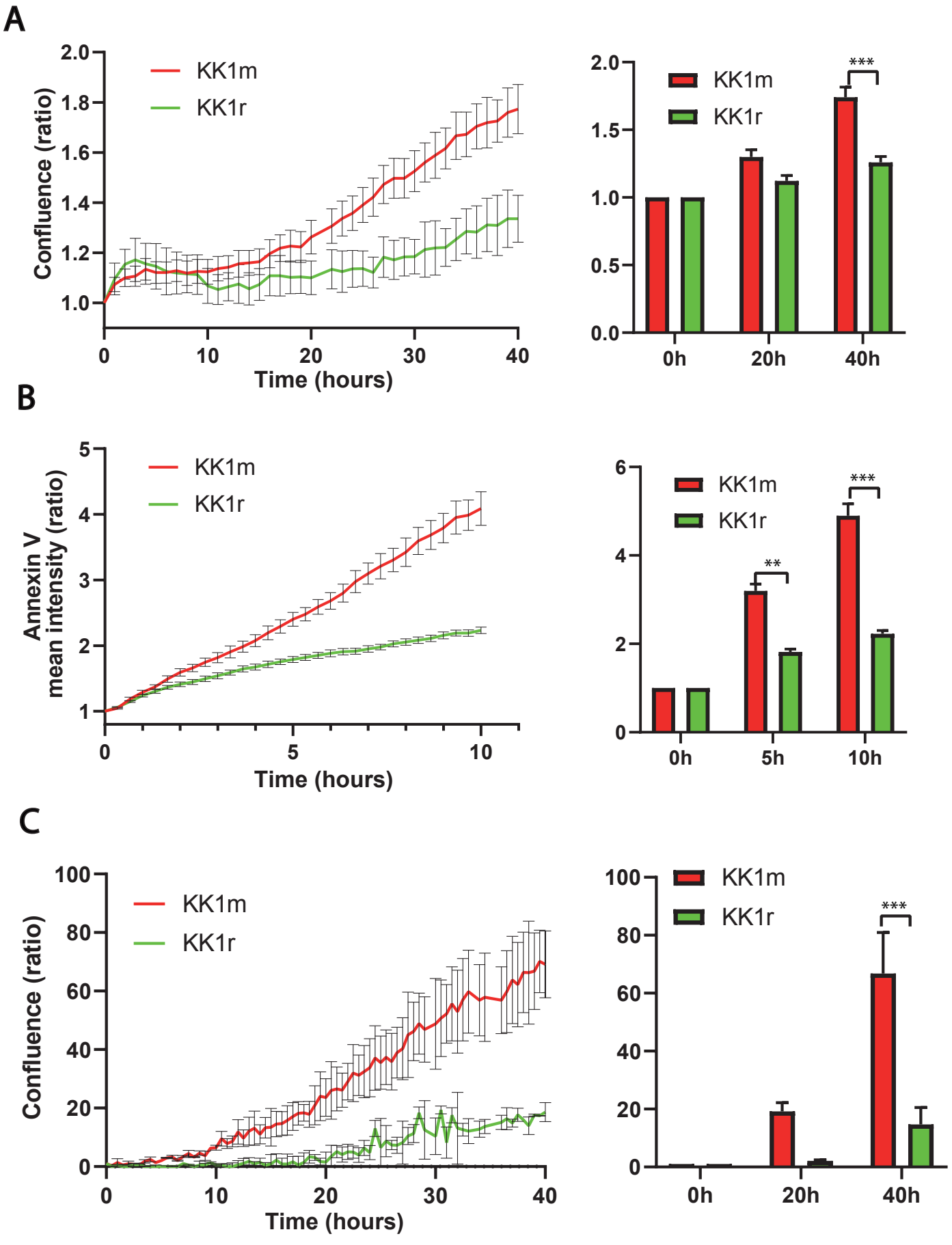
A
Confluence (ratio)
KK1m
KK1r
Time (hours)
***
0h
20h
40h
B
Annexin V
mean intensity (ratio)
**
5h
10h
C
KK1m
KK1r

Figure 2

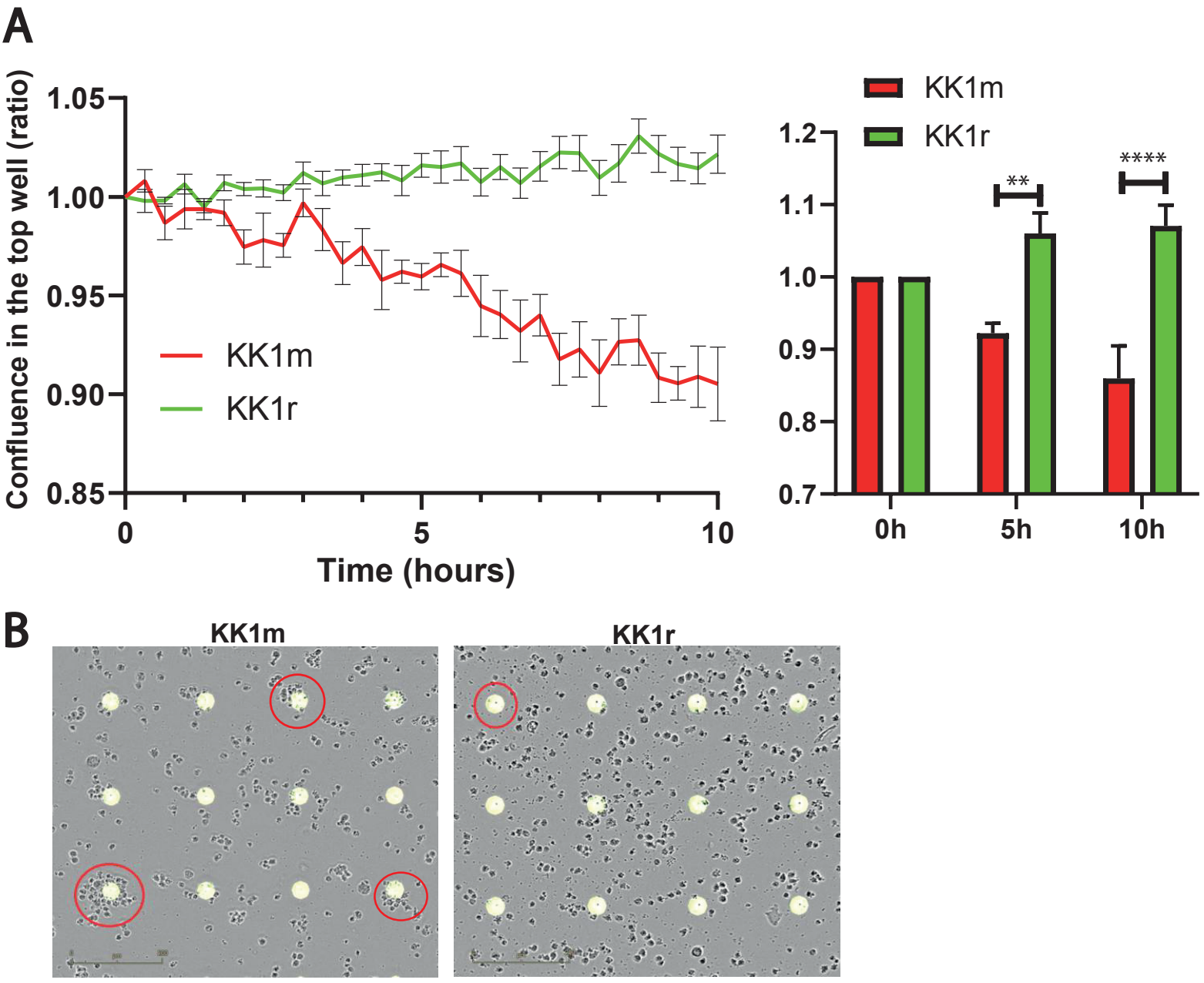
A
Confluence in the top well (ratio)
1.05
1.00
0.95
0.90
0.85
0
5
10
Time (hours)
KK1m
KK1r
KK1m
KK1r
1.2
1.1
1.0
0.9
0.8
0.7
**
****
0h
5h
10h
B
KK1m
KK1r

Figure 3

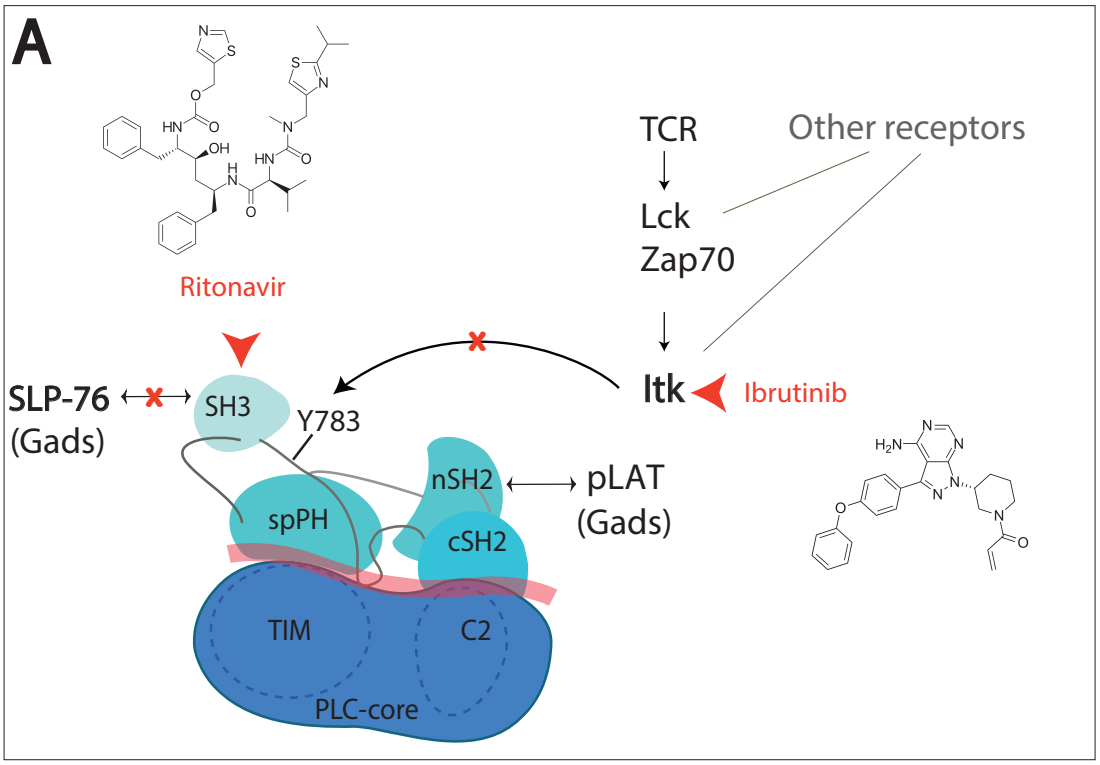
A
Ritonavir
TCR
Other receptors
Lck
Zap70
Itk
Ibrutinib
SLP-76
(Gads)
SH3
Y783
nSH2
pLAT
(Gads)
spPH
cSH2
TIM
C2
PLC-core

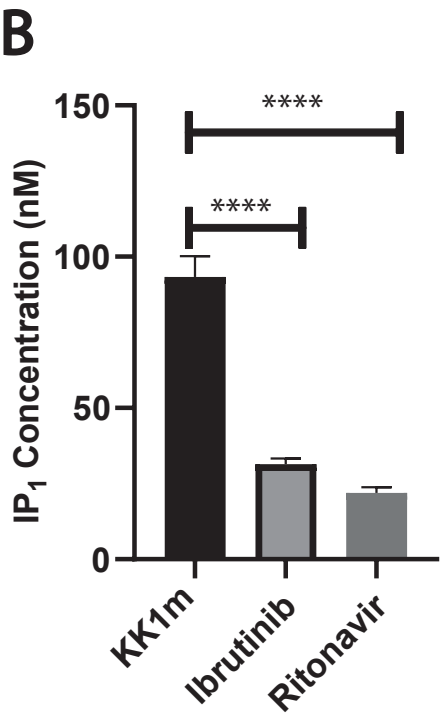
B
IP1 Concentration (nM)
150
100
50
0
****
****
KK1m
Ibrutinib
Ritonavir

Figure 4

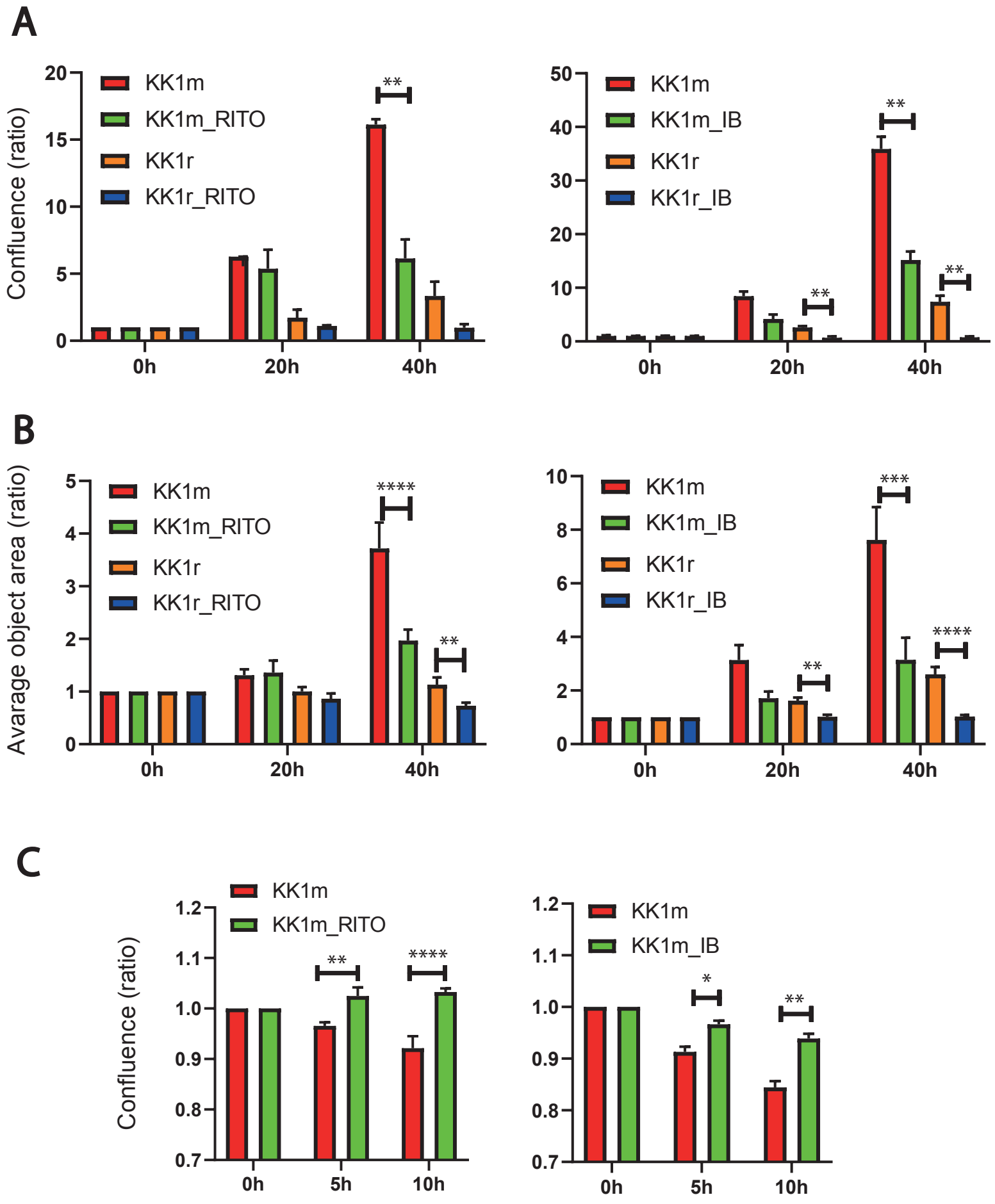
A
Confluence (ratio)
KK1m
KK1m_RITO
KK1r
KK1r_RITO
KK1m_IB
KK1r_IB
0h
20h
40h
B
Avarage object area (ratio)
C
Confluence (ratio)
5h
10h

Figure 5